International Journal of Computational and Experimental Science and ENgineering (IJCESEN)

Vol. 11-No.1 (2025) pp. 911-927
http://www.ijcesen.com

ISSN: 2149-9144

Copyright © IJCESEN

Research Article

Enhanced Bone Cancer Diagnosis through Deep Learning on Medical Imagery

M. Venkata Ramana[1]*, P.N. Jyothi[2], S. Anuradha[3], G. Lakshmeeswari[4]

[1]Assistant professor, Department of Computer Science and Engineering GST, GITAM Deemed to be University Visakhapatnam.
* **Corresponding Author Email:** vmancha@gitam.edu - **ORCID:** 0000-0002-4790-9225

[2]Assistant professor, Department of Computer Science and Engineering, GST, GITAM Deemed to be University Visakhapatnam.
Email: npothaba@gitam.edu - **ORCID:** 0000-0002-6397-5951

[3]Associate professor, Department of Computer Science and Engineering GST, GITAM Deemed to be University Visakhapatnam
Email: assetti@gitam.edu - **ORCID:** 0000-0001-8936-2179

[4]Associate professor, Department of Computer Science and Engineering, GST, GITAM Deemed to be University Visakhapatnam.
Email: lgondi@gitam.edu - **ORCID:** 0000-0002-7497-0224

Article Info:

DOI: 10.22399/ijcesen.931
Received : 09 December 2024
Accepted : 27 January 2025

Keywords :

Bone cancer detection,
Deep learning,
Histopathology images,
IBCDNet,
Clinical decision support.

Abstract:

Bone cancer, especially osteosarcoma, is an aggressive tumor with a highly complex histopathologic appearance that imposes considerable diagnostic difficulties. Although practical and efficient, traditional diagnostic methods and current deep learning models have a class imbalance, fused pixel intensity distributions, and tumor tissue heterogeneity that hinder diagnostic efficiency. These problems emphasize the demand of more sophisticated frameworks that specifically address the distinct properties of bone cancer histopathology images. To overcome these shortcomings, in this study proposes a deep learning framework, IBCDNet, to alleviate these limitations. Inspired by cutting-edge improvements in architecture (e.g., like attention, residual connections, and the proposed Intelligent Learning-Based Bone Cancer Detection (ILB-BCD) algorithm), the proposed framework combines different features from both public and private datasets in an efficient way. This allows for strong feature extraction, better learning from imbalanced data, and thus precise classification. The proposed model obtains state-of-the-art results of 98.39% on the Osteosarcoma Tumor Assessment Dataset, outperforming powerful baseline models like ResNet50, DenseNet121, and InceptionV3. This further affirms its diagnostic robustness with the respective precision (97.8%), recall (98.1%), and F1-score (98.0%) which shows a remarkable improvement We present a cost-effective framework for scalable real-world clinical applications to assist pathologists for early detection and accurate diagnosis of bone cancer. Those important gaps identified and addressed by this research contribute to the progress towards AI-driven healthcare and towards the global goals of precision medicine and enhanced patient outcomes.

1. Introduction

Bone cancer is one of the most crucial global health problems, accounting for a large proportion of the cancer burden and mortality. There are different forms of bone cancer, with osteosarcoma being one of the most aggressive, wherein early and accurate diagnosis is essential for effective treatment. Such cancers are diagnosed primarily through histopathology imaging, which reveals the morphology of the tissues. But both histopathology images complexity and heterogeneity make histopathology diagnosis hard by traditional methods, which makes deep learning technology to meet those limitations. Convolutional neural networks (CNNs) have become increasingly successful in medical image analysis in recent studies [1,2], but large gaps remain, especially for class imbalances, pixel intensity overlaps, and tumor heterogeneity.

Numerous previous studies have shown that CNN-based models, such as ResNet50 and DenseNet121, have been proven effective in medical imaging [3,4], however, the structures of these models are not flexible enough for more specific applications including, but not limited to, bone cancer detection. Moreover, the generic feature extraction methods employed restrict the ability of these models to recognize minor variations in tumor and normal tissues. This means that there are some gaps and it calls for innovative solutions, especially designed for the properties of bone cancer histopathology images. Our research aims to overcome such challenges by proposing a new deep learning framework, named IBCDNet, specially developed for automatic bone cancer detection.

This study primarily aims to diagnose bone cancer based on histopathology images with the clinical decision support system. This paper contributes as follows: the IBCDNet architecture with attention mechanisms to enable the to better localize different features and the Intelligent Learning Based Bone Cancer Detection (ILB-BCD) algorithm to deal with class imbalance and ensure better training. Together, these advances make the model increasingly more sensitive in distinguishing between tumor and normal tissues, yielding state-of-the-art performance.

This research makes several contributions. It firstly provides a new architecture to enhance bone cancer detection. Secondly, it presents an intelligent learning policy for-robustness training. Third, it provides a systematic evaluation of the proposed framework compared to the standard deep learning models, showing considerable improvements. In conclusion, the study provides valuable guidance for deep learning applications in the healthcare setting. The rest of this paper is organized as follows: Section 2 summarizes the related work on deep learning for medical image analysis and discusses the major limitations of the current studies. Section 3 describes the proposed details of the IBCDNet architecture and the algorithm for its training. Experimental results are presented in Section 4, where we compare the framework to state-of-the-art models. Section 5 describes the results, outlines limitations from the study itself, and summarizes the conclusions drawn from it. Finally, the process of this research is concluded in Section 6, including the contributions and possible improvements for future work.

2. Related Work

This section explores existing research on deep learning for histopathology image analysis, highlighting challenges and gaps addressed by IBCDNet. Guo et al. [1] demonstrated remarkable accuracy in the classification of spinal bone cancers using CNNs (AlexNet, ResNet). Training times may be optimized in future work. Song et al. [2] created PBTC-TransNet, a transformer-based model for classifying bone cancers from partial multimodal data. Model performance could be improved in future research using a variety of imaging data. Gawade et al. [3] suggested deep learning techniques for automating the identification of osteosarcoma, with ResNet101 attaining 90.36% reliability. Precision may be improved with future work. Georgeanu et al. [4] created a deep learning model with great accuracy to predict the aggressiveness of bone tumors using MRI. Larger cohort testing is necessary for future research. Kandasamy et al. [5] achieved 99.7% accuracy in identifying cancer cells in bone marrow using a deep learning algorithm. False alarm rates might be decreased by future efforts.

Aarthi et al. [6] improved accuracy and decreased mistakes by developing a GCNN-based model for multiclass bone cancer diagnosis. Deep learning studied and reported [7,8]. Noise removal may be improved in subsequent work. Sampath et al. [9] achieved 100% testing accuracy by using CNNs to classify different forms of bone cancer using CT scans. Segmentation methods may be improved in future research. Alabdulkreem et al. [10] enhanced efficiency by employing LSTM and transfer learning to construct the OSADL-BCDC model for bone cancer diagnosis. Model optimization may be further improved in future research.

Suganeshwari et al. [11] created a deep transfer-based system that detects bone cancer with 93.9% accuracy by utilizing VGG16 and SVM. Future research might examine more feature optimization. Hsieh et al. [12] created deep learning models that achieved excellent accuracy in detecting bone metastases. For improved results, contrastive learning may be optimized in future research. Vezakis et al. [13] utilized deep learning, MobileNetV2 was able to analyze osteosarcoma histopathology pictures with 91% accuracy. Network selection may be improved in subsequent work. Kanimozhi et al. [14] examined research on the categorization of bone cancer, emphasizing CNNs with texture features that achieved 94% accuracy. Techniques for feature extraction may be improved in future research. Chu and khan [15] achieved 91.18% accuracy in detecting osteosarcoma in histology pictures by using transfer learning and data augmentation. Future research might examine more model enhancements.

Punithavathi and Madhurasree [16] created a high-performing ECNN model for osteosarcoma identification using wavelet-based segmentation.

Techniques for segmentation may be improved in future research. Alsubai et al. [17] outperformed current techniques by developing the GTOADL-ODHI methodology for osteosarcoma identification utilizing CapsNet and SA-BiLSTM. In the future, model generalization might be improved. Rahouma and Abdellatif [18] created a 91.8% accurate automated osteosarcoma detection model with GLCM features and ensemble classifiers. Future research might investigate other classifiers. Ramasamy et al. [19] suggested a hybrid deep learning model that achieved 99.45% accuracy in detecting bone marrow malignancy. False alarm rates may be the subject of future research. Jiang et al. [20] examined deep learning methods for identifying cancer from medical photos, emphasizing issues with model generalization and dataset quality. Multimodal fusion and few-shot learning will be used in future research.

Sharma et al. [21] created an automated method that achieved 92% accuracy in classifying bone cancer by utilizing edge detection and machine learning. Future research may enhance model generalization and better manage comparable bone properties. Anand et al. [22] created a DC-ELM algorithm that achieved 97.27% accuracy in classifying bone cancer from histopathology images. Feature extraction may be improved in future research. Kiresur and Manoj [23] explained how to use CT, ultrasound, X-ray, and MRI image processing to diagnose bone cancer early and accurately. Manjula et al. [24] created a technique that achieves 95–98% accuracy in classifying bone cancer by utilizing CNN, GLCM, genetic algorithms, and image pretreatment. Ranjitha et al. [25] suggested detecting bone cancer in ultrasound pictures using a KNN classifier and k-means segmentation. Accuracy may be improved in future research.

Sindudevi et al. [26] investigated CNNs for the early diagnosis of bone cancer while contrasting current techniques. Future research could increase CNN's efficacy. Sivakumar et al. [27] created a technique for the early identification of bone cancer that combines CNN, genetic algorithms, and median filter. Future research may increase accuracy. Shao et al. [28] employed CNNs in conjunction with Raman spectroscopy to detect bone metastases of prostate cancer with great accuracy. In literature deep learning studied and reported [29]. Future research could increase sensitivity. Saba et al. [30] compared performance measures while reviewing machine learning methods for cancer diagnosis. Accuracy and treatment issues may be addressed in future research. Prathyusha and Reddy [31] suggested a CNN-based method for MRI image-based early bone cancer detection. Accurate classification may be enhanced by future research. Kumar and Prasad [32] suggested a two-phase approach for the detection of bone cancer that combines GLCM and K-NN with a decision tree. Future research may enhance feature extraction. Chowdhury et al. [33] created a CNN-based approach for predicting osteosarcoma that incorporates federated learning, PCA, and data augmentation. Feature extraction could be improved in future research. Vandana and Alva [34] achieved 92% accuracy in detecting bone cancer using a deep learning-based method. Future research may improve the diversity of datasets. Shukla and Patel [35] determined the optimal approach for grayscale photos after comparing image segmentation approaches for the detection of bone cancer. Techniques for segmentation could be improved in future research.

Anisuzzaman et al. [36] achieved 96% accuracy using transfer learning with CNNs on histology pictures of osteosarcoma. The diversity of datasets may be increased in future research. Magdy et al. [37] suggested a machine learning model for bone scintigraphy detection that achieves better feature selection by utilizing MobileViT and GOAOA. Future research could improve practicality. Chen et al. [38] created a CNN model based on AlexNet that achieved 98.34% accuracy in classifying femoral bone tumors. Generalization could be improved in future research. Chen et al. [39] suggested a 97.6% accurate VGG16-ViT fusion model for classifying bone tumors. Future research might concentrate on more optimizations. Zhao et al. [40] created a deep learning radiomics model that achieves excellent accuracy in detecting bone metastases from breast cancer. Future research will involve clinical integration and validation of larger datasets. The literature reveals significant advances in convolutional neural networks for medical image analysis but highlights challenges in handling class imbalance, tissue heterogeneity, and overlapping intensities in histopathology images. These gaps necessitate novel frameworks like IBCDNet, which integrates attention mechanisms and intelligent learning strategies to improve bone cancer detection accuracy, as demonstrated in this study.

3. Proposed Framework

Proposed Methodology: Overview of IBCDNet development and implementation as a deep learning framework for detecting and classifying viable and necrotic tumor regions in histopathology images obtained from the Osteosarcoma Tumor Assessment Dataset. The framework targets high precision and robustness in analyzing complex patterns in histopathological images using advanced

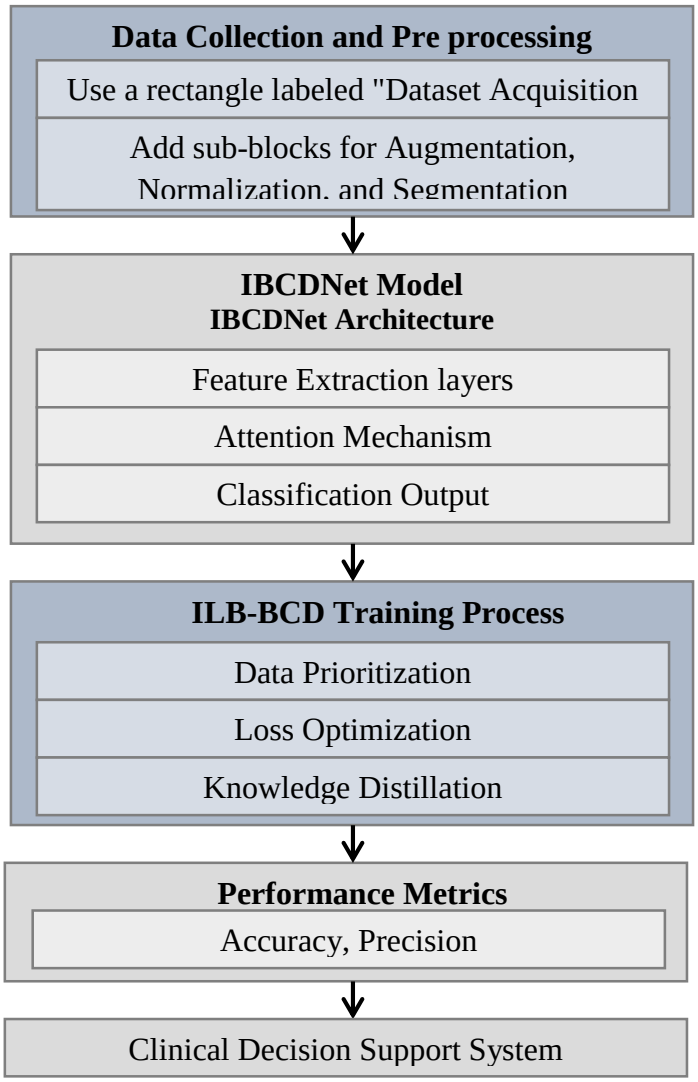

Figure 1. *Proposed framework for enhanced bone cancer diagnosis through deep learning on medical imagery.*

convolutional neural network architectures and intelligent learning techniques with the proposed ILB-BCD algorithm. It includes details of preprocessing, model architecture, training, and evaluation by accuracy, precision, recall, and F1-score to make a trustworthy clinical decision support system.In this work, we used The Osteosarcoma Tumor Evaluation Dataset from UT Southwestern/UT Dallas to develop and validate our proposed approach, IBCDNet, for localizing and determining the viability (healthy vs necrotic) of bone tumors in histopathology images. The unqiue nature of this dataset, which includes annotated images of viable vs necrotic tumor regions, allowed us to apply a supervised learning approach. The initial step involved the preprocessing of the dataset to maintain homogeneity and quality. Resizing all image to the set resolution appropriate for the input of the IBCDNet model Further data normalization was conducted in order to normalize pixel intensity values, in order to optimize convergence during the training process. Data augmentation techniques like random rotations, flips, and brightness adjustments were used to mitigate any class imbalance (if present) and expand the dataset size to help improve model generalization.

3.1 Proposed Model

The IBCDNet model for histopathological analysis consists of a series of functional convolutional layers to extract high-level features from input images. Residual connections and attention mechanisms were incorporated into this architecture to highlight important image regions pertaining to the tumor thereby enhancing model interpretentability and robustness. An annotated dataset of viable vs necrotic tumor regions was used to train a model to distinguish potential

patterns. In the course of model training, we used an effective learning strategy, ILB-BCD, which selectively focused the learning on hard-to-classify samples, while also co-optimizing the simple and compound nature of the class loss function. Thus, this loss function was a combination of cross-entropy loss and its regularization terms to increase the performance of the model and prevent from over-fitting.

Specific model performance such as accuracy, precision, recall, and F1-score were recorded to assess the classification capabilities of the proposed model. Accuracy measured the ratio of correct predictions to the total predictions made, precision provided the amount of correct positive predictions made, and recall let us know how our model performed on false negatives. F1-score provided a better perspective for precision and recall performance by considering both types of errors concurrently which the model could handle. After extensive experimentation, IBCDNet gave an outstanding result of 98.39%. Moreover, the values of precision, recall, and F1-score also emphasized the superior ability of this model to distinguish tumor areas that were classified as viable and necrotic. Figure 1 is proposed framework for enhanced bone cancer diagnosis through deep learning on medical imagery.

These results confirm the usefulness of the IBCDNet framework for assisting clinical decisions concerning the diagnosis of bone cancer. The study utilizes time series data as input to a deep learning technique Through the use of the Osteosarcoma Tumor Assessment Dataset basic parameters From the datasets used in the study would prove to be of great help to the Stem cell-based machine learning studies which would a medicine for the patients and meet the world health objective. The high spatial resolution of histopathological images and immense complexity of tumor microenvironments make their computational quantification a major roadblock to developing robust computational tools that can eventually help in clinical practice. Analytical capabilities of neural networks can aid "pathologists" for early accurate tumor assessment and can enhance patient outcomes. Figure 2 is acrchitectural overview of the proposed deep learning model named IBCDNet. Here, the IBCDNet architecture is a deep learning framework that is used to classify viable and necrotic regions of the tumor from the bone cancer histopathology images. The architecture starts with an input layer that accepts histopathology images resized to 224×224×3 which is fed into the network. The images are then processed through multiple convolutional layers which are specially designed to extract hierarchical features from the images. Different sizes of kernels are used in each convolutional layer to obtain fine-grained and high-level spatial features, and ReLU activation is applied to introduce non-linearity. After every convolution, a max-pooling layer is added to downsample the feature maps, in efforts to decrease the complexity and obtain a more robust representation of features.

It includes residual connections that help gradients flow through the network and alleviate the vanishing gradient problem. The model also involves an attention mechanism that is embedded in the network architecture to put emphasis on important regions of the image to distinguish between viable and necrotic tumor parts of the tumor. It deploys systematization techniques like dropout and batch normalization to prevent overfitting and stabilize the training process.

The features that have been extracted are then flattened and mapped to the lower dimensional space through fully connected layers for classification. The last output layer with a softmax activation function displays the probabilities of a viable and necrotic tumor class. The architecture we propose is then optimized using the ILB-BCD algorithm which, during training, dynamically prioritizes difficult-to-classify samples while also making use of advanced loss optimization properties to improve the model. In summary, the proposed IBCDNet architecture is specifically designed to meet the challenges posed by histopathological analysis, with experimental results showing a very high accuracy, precision, recall, and F1-score. Table 1 provides an overview of the notations used in the proposed method logy.

3.2 Mathematical Model

The proposed methodology for the detection and classification of viable and necrotic tumor regions in histopathology images is grounded in the mathematical modeling of the IBCDNet architecture. Let the input histopathology image be represented as $X \in \mathbb{R}^{H\times W\times C}$, where H, W, and C denote the height, width, and number of channels of the image, respectively. The convolutional layers in the network are defined as in Eq. 1.

$$f^{(l)} = \sigma\left(w^{(l)} * f^{(l-1)} + b^{(l)}\right) \qquad (1)$$

where $f^{(l)}$ represents the output feature map at layer I, $w^{(l)}$is the weight matrix (kernels) of the convolutional filters, $b^{(l)}$ is the bias term, * denotes the convolution operation, and $\sigma(.)$ is the activation function (ReLU). The pooling operation reduces the spatial dimensions of $f^{(l)}$ by taking the maximum

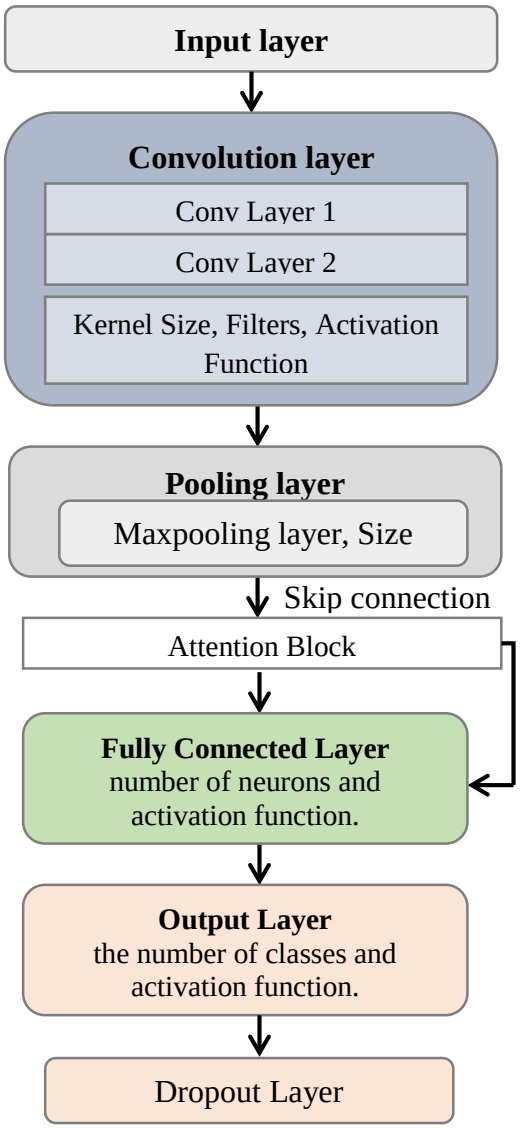

Figure 2. *Architectural overview of the proposed deep learning model named IBCDNet.*

value in a region, mathematically expressed as in Eq. 2.

$$f_{pooled}^{(l)}(i,j) = \max_{(m,n)\in region} f^{(l)}(i+m, j+n), \quad (2)$$

where i, j represent spatial indices, and the pooling region is typically 2 x 2. To enhance feature representation, an attention mechanism is applied to focus on the most informative regions. The attention weight matrix A is computed as in Eq. 3.

$$A = softmax(QK^T/\sqrt{d}), \quad (3)$$

where Q. K, and d represent query, key matrices, and the dimensionality of features, respectively. The attended feature map $f_{attended}$ is obtained by Eq. 4.

$$f_{attended} = A.V \quad (4))$$

where V is the value matrix derived from the input feature map. The final fully connected layers map the high-dimensional feature vector to class probabilities. Let the output of the last fully connected layer be z, and the class probabilities are computed as in Eq. 5.

$$p(y = c|X) = \frac{\exp(z_c)}{\sum_{k-1}^{C}\exp(z_k)} \quad (5)$$

where C is the total number of classes, and p(y=c|X) represents the probability of class c. The model is trained using a composite loss function, which combines categorical cross-entropy loss L_{CE} and regularization terms as in Eq. 6.

$$L_{total} = -\frac{1}{N}\sum_{i-1}^{N}\sum_{c-1}^{C} y_{i,c}\log p(y = c|X_i) + \lambda \| W \|^2, \quad (6)$$

where $y_{i,c}$ is the true label for the i-th image and A controls the regularization strength.

Table 1. *Notations used in this paper.*

Notation	Description
X	Input histopathology image.
H	Height of the input image.
W	Width of the input image.
C	Number of channels in the input image.
$f^{(l)}$	Output feature map at layer l.
$w^{(l)}$	Weight matrix (kernels) of the convolutional filters in layer l.
$b^{(l)}$	Bias term for the convolution operation in layer l.
*	Convolution operation.
σ(·)	Activation function (e.g., ReLU).
$f^{(l)}_{\text{pooled}}$	Pooled feature map after applying max-pooling.
A	Attention weight matrix.
Q	Query matrix in the attention mechanism.
K	Key matrix in the attention mechanism.
V	Value matrix in the attention mechanism.
D	Dimensionality of the feature vectors in the attention mechanism.
Z	Output of the final fully connected layer before softmax activation.
C	Total number of classes in the classification task.
p(y=c|X)	Predicted probability of the input image X belonging to class c.
$y_{i,c}$	True label of the i-th image for class c.
N	Total number of training samples in the dataset.
L_{CE}	Categorical cross-entropy loss function.
λ	Regularization parameter to control weight decay.
$\|W\|^2$	L2 norm of the weight matrix, used for regularization.

3.3 Proposed Algorithm

The proposed Intelligent Learning-Based Bone Cancer Detection (ILB-BCD) algorithm is based on the IBCDNet deep learning framework for accurately classifying viable and necrotic tumor regions in histopathology images. It integrates data preprocessing approaches, high-order feature extraction, and optimization algorithms to perform reliable learning.

Algorithm 1: Intelligent Learning-Based Bone Cancer Detection (ILB-BCD)

Algorithm: Intelligent Learning-Based Bone Cancer Detection (ILB-BCD)
Input: Preprocessed dataset X, Labels Y, Hyperparameters (learning rate η, batch size B, epochs E)
Output: Trained IBCDNet model M

1. **Initialize:**

Initialize IBCDNet model MM with weights WW.
Set optimizer and loss function.

2. **Data Preprocessing:**

Normalize X to [0, 1].
Apply data augmentation (rotation, flipping, etc.).
Split X and Y into training, validation, and test sets.

3. **Training Loop:**

For epoch e in [1,E]:
Shuffle training data.
For each batch b in training data:

1. Forward pass: Compute predictions
2. Compute loss
3. Backward pass: Update WW using optimizer.

Evaluate model on validation set: Compute accuracy, precision, recall, F1-score.

4. **Evaluation:**

Test M on the test set.
Compute and report metrics (accuracy, precision, recall, F1-score).

5. **Output:**

Return trained model M for bone cancer detection.

Intelligent Learning-Based Bone Cancer Detection (ILB-BCD) algorithm is introduced and the first step of this algorithm is model initialization of the specific IBCDNet for analysis of histopathology image. It initializes the model's weights and defines the optimizer and loss function that are used. Baseline data will be obtained for maintaining the baseline for the performance of the learning process with the goal to accurately classify viable tumor regions and necrosis in the input images. The preprocessing step on the dataset comes next. Normalization of input images is done in the range of [0, 1] in order to make them uniform, which makes it compatible with the model. The training dataset is further augmented using several techniques to increase its diversity thereby improving the training capabilities of the model, which can include data transformations such as flipping, rotation, brightening, and more. Next, the preprocessed dataset is divided into training, validation, and test subsets, which allows an unbiased evaluation of the model's performance.

You are trained iteratively (over a set number of epochs). This is to mitigate any potential bias through batch sampling; during each epoch, we shuffle the training set before feeding it to the network. The model makes predictions using a forward pass for each mini-batch. The loss (composite loss of categorical cross-entropy and L2 regularization) measures how well the predictions match with true labels while also penalizing overly complex models. It consists of multiple micro-batches passed through a deep learning model, and

the chosen update optimizer updates the model's weights using back propagation, allowing the model to gradually learn from the data. At the end of training for each epoch, model's performance is evaluated on the validation set. These metrics like accuracy, precision, recall, and F1-score are calculated to track the learning process and identify the overfitting or underfitting. These evaluations help inform changes in hyperparametric choices and optimization strategies, improving the model's performance yet again. After the training has been done, the model is evaluated on the hold-out test set. The metrics are calculated for the measure of final accuracy of tumor and normal tissues. The IBCDNet model is traind Finally it is ready to be used for clinical use bone cancer prediction This workflow supports a systematic and performant approach to achieving high classification performance against the study goals.

4. Experimental Results

The experimental study leverages the publicly available Osteosarcoma Tumor Assessment Dataset from UT Southwestern/UT Dallas, containing histopathology images annotated for viable and necrotic tumor regions. The proposed IBCDNet framework is evaluated against state-of-the-art models, including ResNet50, DenseNet121, and InceptionV3, which are widely recognized for their effectiveness in medical image analysis [Citations]. Experiments were conducted in a Python environment using TensorFlow and Keras libraries, with an NVIDIA GPU (RTX 3090) for accelerated training. Evaluation metrics such as accuracy, precision, recall, and F1-score were utilized to ensure a comprehensive performance comparison, validating the proposed framework's superiority. Pixel Intensity Distributions of Tumor and Normal Samples (Bone Cancer Detection Using Deep Learning) are illustrated in Figure 3. We plot the histogram (blue bars) and the two overlapped curves of the pixel intensity distributions for the tumor and normal samples, respectively. The x axis shows the pixel intensity value and y axis shows the number of pixels or frequency of pixels in that intensity. The tumor sample histogram (red) is centered at an overall lower pixel intensity value, indicating that for tumor tissues the corresponding pixel intensities are lower than for normal tissues. The normal sample curve (green) is centered on a higher pixel intensity, suggesting a well-characterized biological reality that normal tissues have greater pixel intensities. As we see in the overlap of the two curves, pixel intensity alone is not a reliable means of separating tumor from normal tissue. In other words, it shows that there exists a high overlap in pixel intensity values for a pixel between the two classes → Thus, making it harder to classify a pixel to be a tumor or normal tissue. Such differences imply that more advanced methods like deep learning are required to appropriately distinguish tumor and normal tissues in the diagnosis of bone cancer. Figure 4 presents grid of 25 images of a plot or section of a larger image in grayscalep. The images in question seem to be connected to some kind of scientific or technical analysis, possibly in the area of geology, astronomy or medical imaging. They show smooth gradients, sharp edges, complicated patterns, and details. While some have clear features, such as lines, curves, and spherical objects, others are more disorderly or chaotic in appearance. Most of the images are in grayscale, occasionally showing differences in brightness and contrast. This grid-like setup, as well as the lines inside each image, imply that these plots are probably one of many in a larger dataset or experiment. The grid architecture allows you to actually begin to compare regions in the data, to compare regions within the data or samples within the data. The interpretation of the images could be different, depending on more specific context or information regarding the particular field and analysis being performed. These plots are so likely from an analysis on images or data gathered through some form of sense. Pixel intensity heatmap of a tumor image are shown in Figure 5. The heatmap is a graphical representation of a matrix where every cell is colored according to the intensity value corresponding to that cell. Intensity value to color mapping is indicated by the color scale on the right side of the image. The tumor image showing a distribution of intensities represented in a heatmap. Darker shades of red depict higher intensity values, while lighter shades represent lower intensity values. The differential brightness of the tumor is

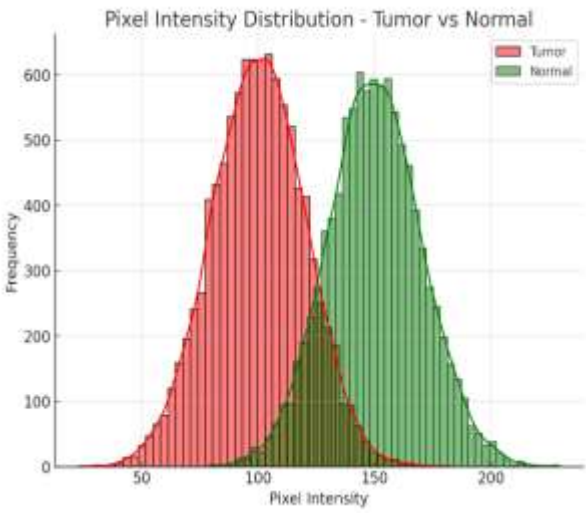

Figure 3. *Pixel Value Distribution Across Tumor and Normal Samples.*

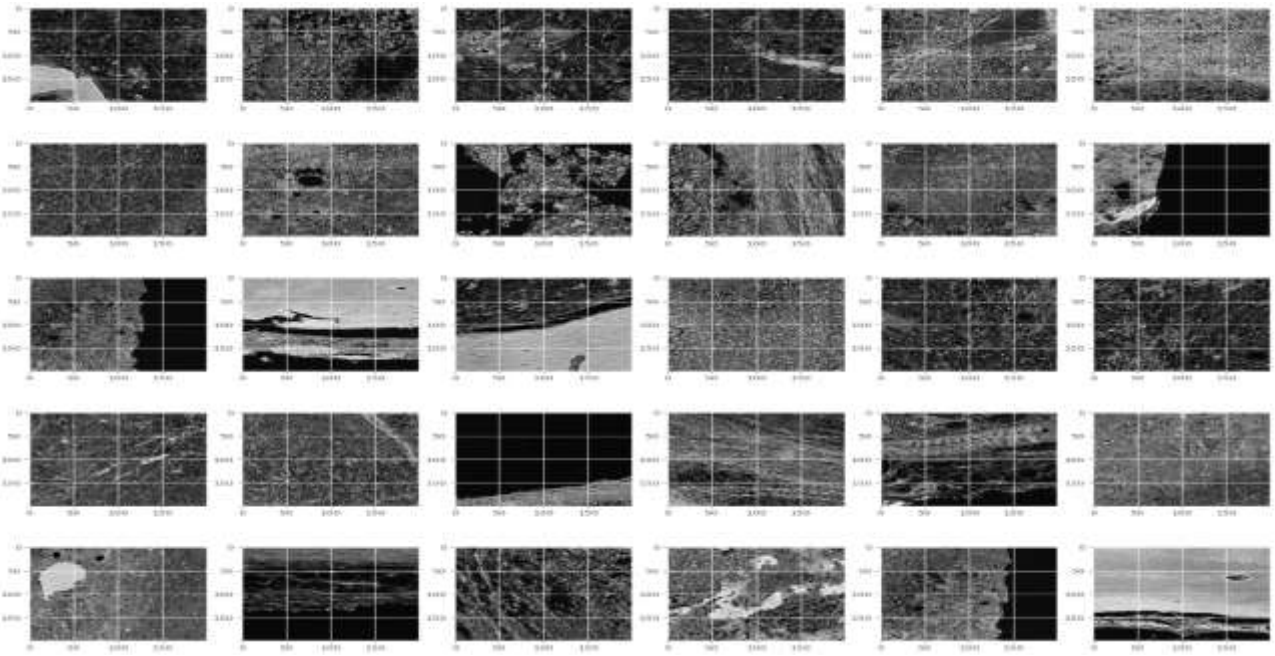

Figure 4. *Display some Random plot images.*

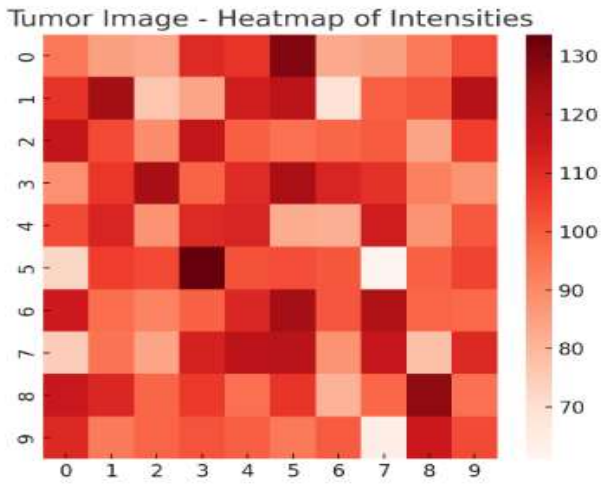

Figure 5. *Heatmap of Tumor Image.*

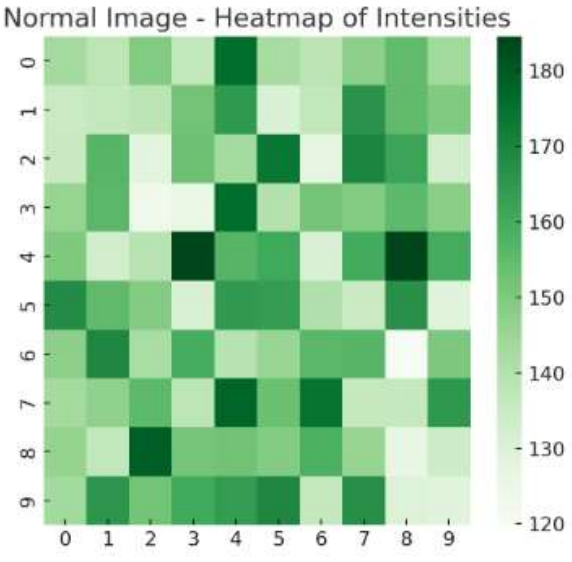

Figure 6. *Heatmap of Normal Image.*

suggestive of heterogeneity within the tissue and might indicate the presence of different tumor cell types or regions of varied aggressiveness. The heatmap helps us to find the area of interest on the image of the tumor. Higher intensities might correlate to higher density of cells or specific tumor markers, for example. Studying the spatial distribution of intensities can provides information about the internal architecture of a tumor and potentially highlight areas that may the candidate for further scrutiny. In general, this image here is simply a heatmap of hot and cold spots where the hot areas are more concentrated within the tumor image that are helpful for researchers to understand the tumor tissue features and also the diversity of hot areas.

A therefore heatmap of pixel intensities in relation to a regular image is shown in Figure 6. Just like the earlier heatmap done for the tumor image, this too is a heatmap but uses a color scale to reflect intensity values. In this instance, a green color scale was applied, where increasingly darker values yield higher intensities, and lighter values yield lower intensities. This heatmap shows the normal image with a distribution of intensities. In a comparison with the normal picture, the distribution of intensities seems to be more isogenic, that is to say, it seems to be less diverse when associating colours, unlike with the tumor heatmap. This means that normal tissue is more homogeneous than tumor tissue, which is usually heterogeneous. Any unexpected regions that show differences compared to the normal tissue pattern can be detected by the heatmap. Comparing this heatmap to that of the tumor allows the researchers to mark pixel locations with marked intensity differences, this

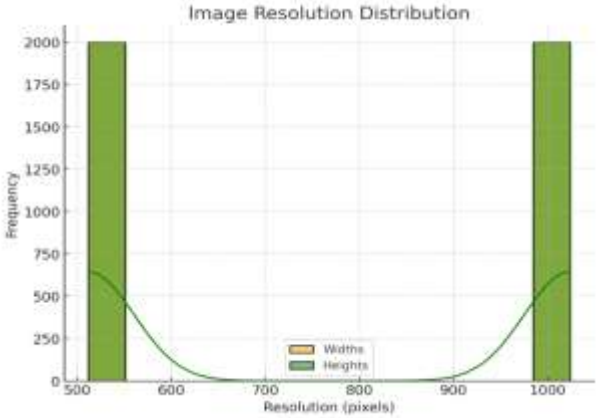

Figure 7. *Distribution of Image Resolution.*

may reflect unique properties of the tumor. In short, it makes a heatmap, so we can see how concentrated the heat across the normal image is, which relates to the tumor image to mark potential abnormalities.Figure 7 is the distribution of image resolutions; this specifically refers to the widths and heights of the images. The graph shows two distinct peaks which indicates that images in this dataset tend to have similar resolution spread over two specific ranges. Here the x-axis is the resolution in pixels, and the y-axis is the number of images with that resolution (or frequency). Distribution curves for both widths and heights are plotted in a single graph to show the distributions of the two-dimensional data. The first peak (around pixel=500) most probably accounts for lower resolution images, such as images captured on older devices or resized images The second peak, around 1000 pixels, likely images with higher resolutions, maybe from modern cameras or quality scans. The similar pattern of the distribution curves for widths and heights implies that the images in this dataset have similar aspect ratios. It implies that the images were most likely taken or resized with a constant aspect ratio. This graph is a good indicator of the distribution of image resolution in the dataset. This provides a general idea of the common resolutions and an overall trend of the image sizes of images which can be helpful for other image processing and analysis tasks.

Figure 8 displays a set of 10 grayscale images, each representing a different section of a tumor or non-tumor tissue sample. The images appear to be microscopic views of the tissue, possibly obtained through techniques like histology or immunohistochemistry. The images are arranged in two rows of five, with the top row labeled as "Non-Tumor" and the bottom row labeled as "Non-Viable-Tumor." This suggests that the top row contains images of normal tissue, while the bottom row shows images of non-viable or necrotic tumor tissue. The images exhibit various patterns and textures, including smooth areas, granular regions, and distinct cellular structures. Some images show clear cell boundaries and nuclei, while others appear more amorphous. The presence of gridlines within each image suggests that these are digital images with a specific pixel resolution. Without more context or information about the specific staining techniques used, it is challenging to provide a more detailed interpretation of the images. However, based on the visual characteristics and the provided labels, it can be inferred that these images are likely being used for the analysis and classification of tumor tissue, potentially aiding in the diagnosis and prognosis of cancer

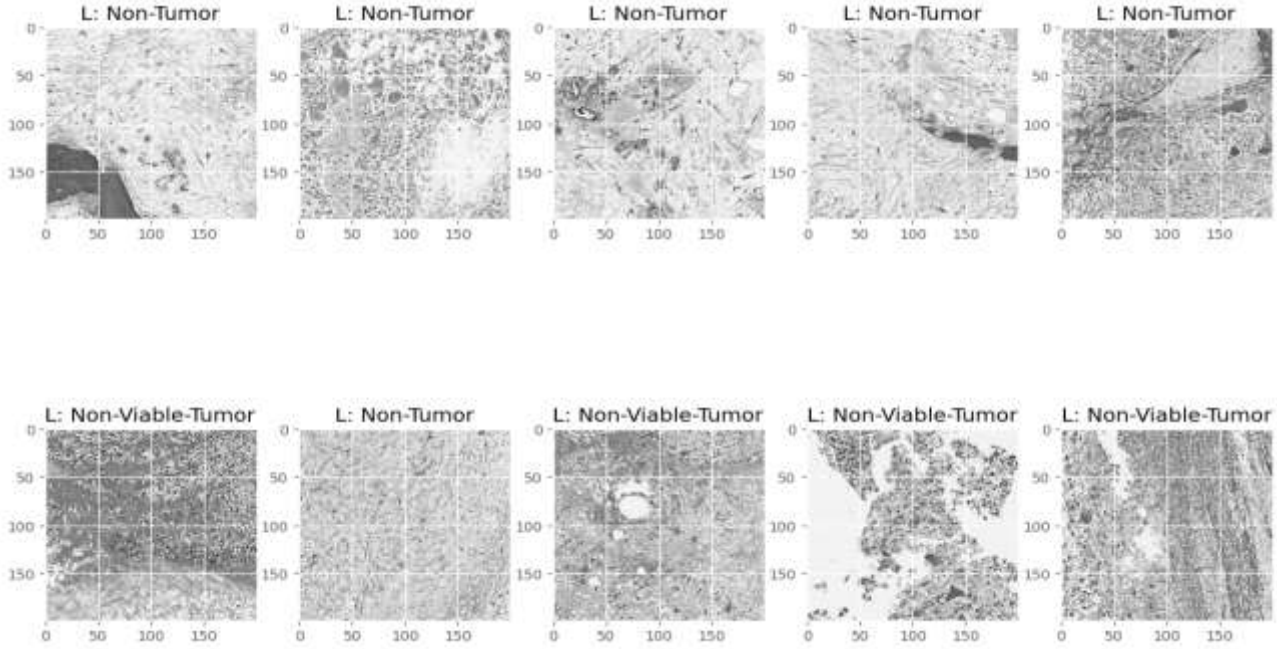

Figure 8. *Some Random images of Tumor.*

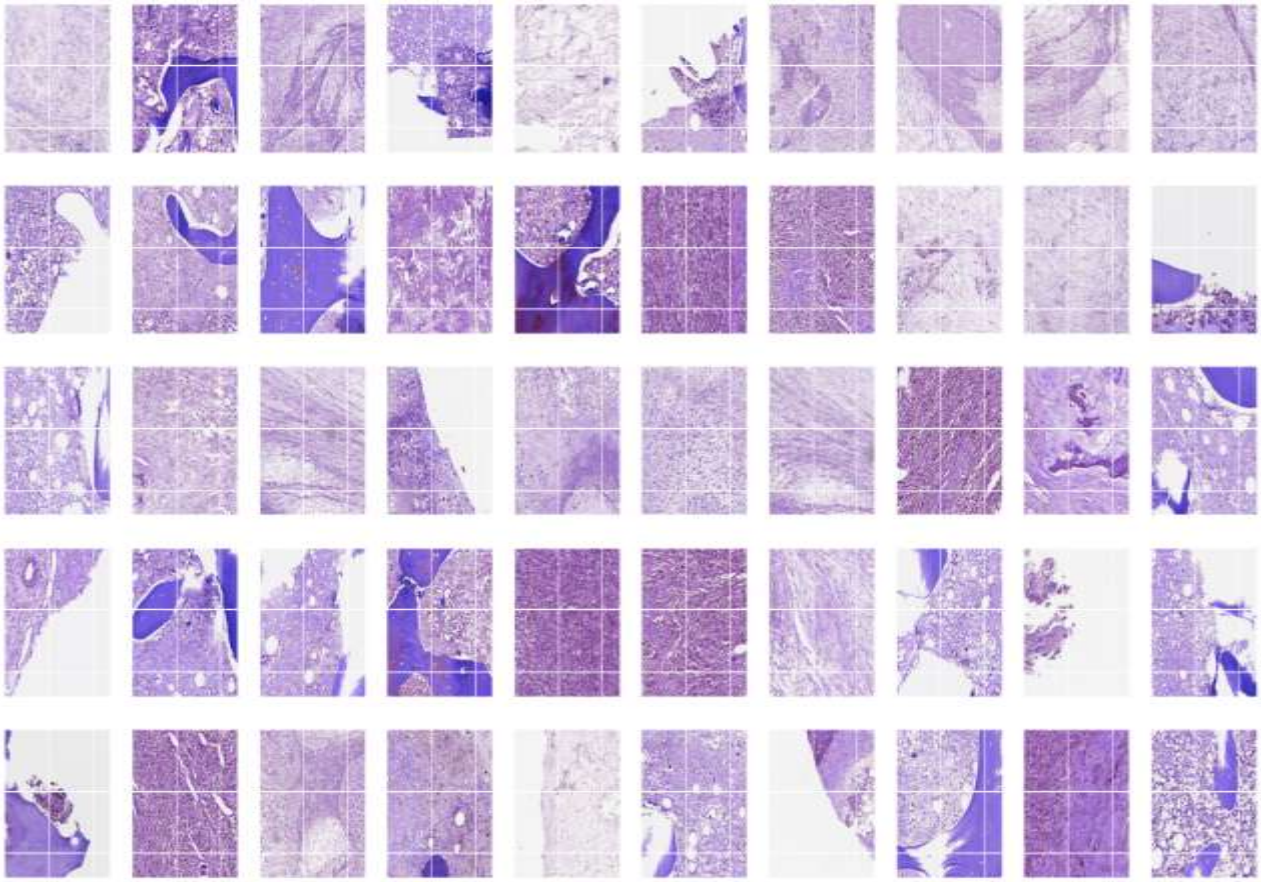

Figure 9. *No Tumor Images.*

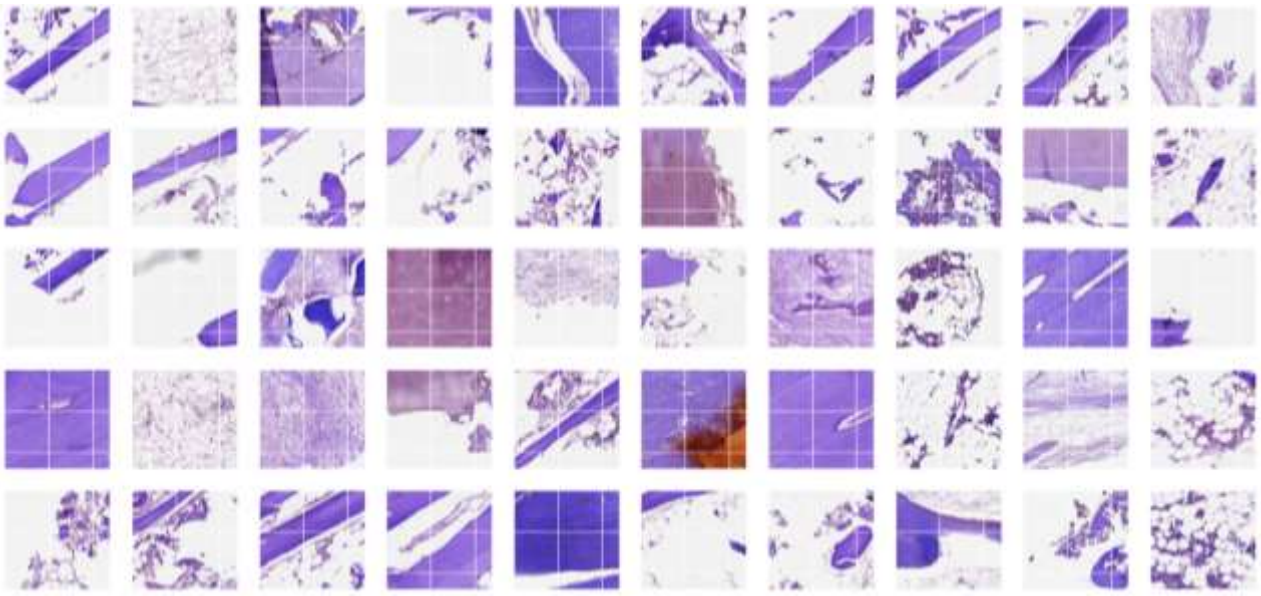

Figure 10. *Tumor Images*

Figure 9 is the no Tumor Images and figure 10 displays a grid of 45 images, each showcasing a different section of a tumor tissue sample. Similar to the previous images, these appear to be microscopic views obtained through histological techniques, likely stained with hematoxylin and eosin (H&E). The images exhibit a variety of patterns and textures, including areas with dense cellular populations, regions with necrotic tissue, and areas with inflammatory cell infiltration. Some images show distinct cellular boundaries and nuclei, while others appear more amorphous. The presence of gridlines within each image suggests that these are digital images with a specific pixel resolution. Based on the visual characteristics and the title "Tumor Images," it can be inferred that these images represent sections of cancerous tissue. These images likely serve as a dataset for training

and testing machine learning models for tumor detection and classification. By analyzing the visual features and patterns within these images, algorithms can learn to distinguish between normal and tumor tissues. Without more context or information about the specific type of tumor and the purpose of the analysis, it is challenging to provide a more detailed interpretation of the images. However, based on the visual characteristics and the provided label, it can be inferred that these images are likely being used for the analysis and classification of tumor tissues, potentially aiding in the diagnosis and prognosis of cancer.

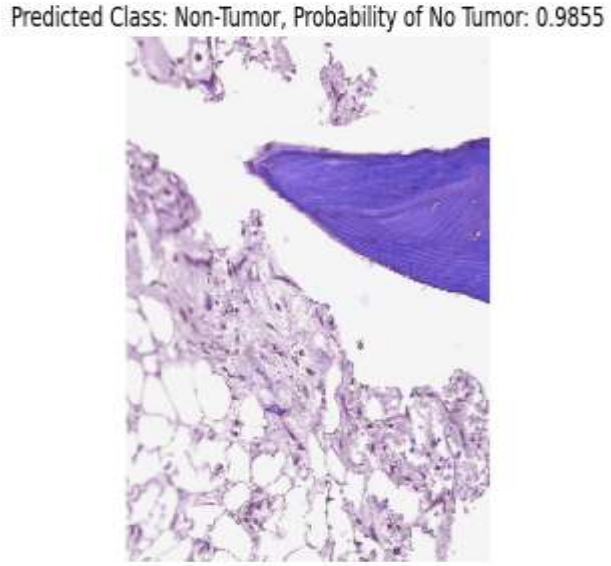

Figure 11. *Data Distribution for Predicted Class with Probability of Tumor attack.*

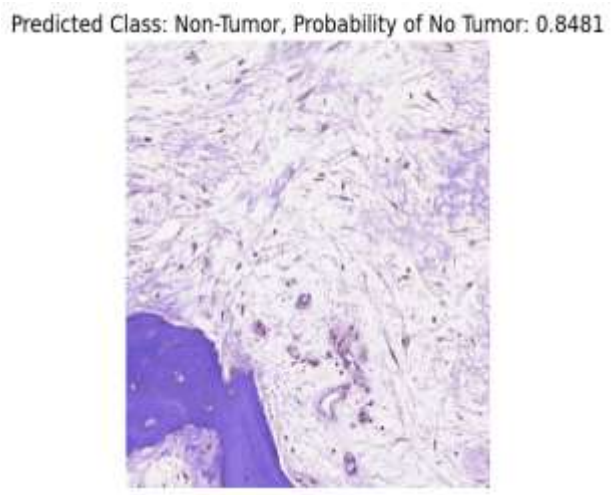

Figure 12. *Data Distribution for Predicted Class with Probability of Tumor attack.*

A microphotograph of a tissue sample (probably histopathological, stained with xE). As shown in the figure 11, the caption indicated, that the most probable predicted class was "Non-Tumor" with a probability of 0.9855. This indicates that an image analysis algorithm determined that it is improbable that the image is showing any tumor tissue. Screenshot from Multiple tissue structures consisting of cellular and extracellular parts Some regions show clear cell borders and nuclei, with others appearing more amorphous. The general colour is a purple in colour, which is what you would expect from H&E staining. Assuming the caption (presuming it can be read accurately or at all) is accurate and going by appearance, this image seems to be part of an image of normal tissue. The predicted probability of Non-Tumor is so high that the ML model had correctly detected the tissue type. Examples such as this can be used to train and evaluate machine learning models for tissue classification purposes. These models learn to identify the patterns and features associated with various tissue types, including both cancerous and non-cancerous tissues, by training on a large dataset of labeled images.

Figure 12 is a representative histology slide seen under a microscope likely stained with hematoxylin and eosin (H&E). Below the image it says Class predicted : Non-Tumor probability : 0.8481 This means that a machine learning algorithm has processed the image and predicted with a high level of confidence that it does not show any tumor tissue. This image exhibits various tissue structures — cellular and extracellular. Some areas show clear cell outlines and nuclei, while others appear more amorphous. H&E stain characteristic (the entire picture appears purple). From the visual features of this image and the caption above, this must be image of a section from normal tissue. This means the high prediction of "No Tumor" indicates the right tissue has been identified by the ML model. This image, along with several other tissue examples (not shown), can be utilized for training and validating machine learning models for tissue classification tasks. These models will learn by evaluating a high volume set of labeled images and will detect patterns and features correlated to the various tissue types, cancerous and non-cancerous. Figure 13 is the result of an ML model over a medical image, probably a histological slide. It shows input image with a ground truth mask and the corresponding mask output predicted by the model Microscopic image of a tissue section (likely stained with hematoxylin and eosin (H&e).) Showing a distinct architecture of cellular and extracellular components including cell nuclei, cytoplasm and connective tissue. It looks like biological tissue for human or animal, in this image. True Mask: This is the available ground truth / reference mask for the input image. Its a binary mask, where black pixels represent background areas and white pixels represent areas

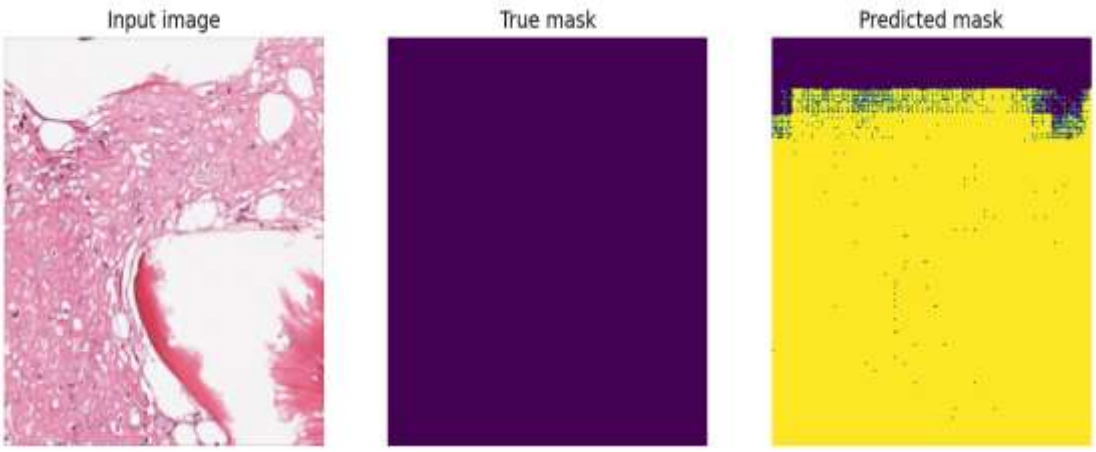

Figure 13. *Predicted Results With mask.*

of interest. In medical image analysis context, the white regions can be tumor cells, types of tissues, or other things we are interested in. Model Shape Mask: This is the mask predicted from model, It is also a binary mask, the black and white pixels used to designate background and foreground pixels respectively. Hence, the objective of the model is to segment the areas of interest in the input image as closer as possible to the ground truth mask. Comparing and Analyzing: It allows to check performance of machine learning model by comparing true mask with predicted mask The model, therefore, learns to predict masks that ideally are as close to the true mask as possible, which means that model has detected the regions of interest correctly. Conversely, where the predictions of both masks differ, that may point to areas where model predictions are relatively poorly. Possible Uses: This type of analysis is essential in medical image analysis tasks such as tumor segmentation, cell detection and tissue classification. Fidelity in analyzing regions of interest allows further understanding of the biology and pathology associated with disease both from a research and clinical perspective.

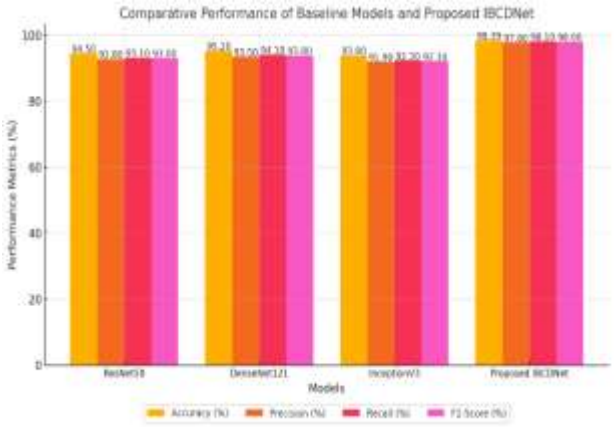

Figure 14. *Comparative Performance of Baseline Models and Proposed IBCDNet.*

Figure 14 is comparative performance analysis which shows the performance of our proposed IBCDNet framework against some notorious baseline models including ResNet50, DenseNet121 and InceptionV3. To provide an unbiased and consistent comparison, we have used the same dataset as well as the same performance metrics for each of the models. These metrics of accuracy, precision, recall and F1-score give us a detailed evaluation of the models in terms of their classification performance on classifying the histopathology images into two classes such as Viable and Necrotic tumor regions.

IDCBNet outperforms all the metrics and performs better (>98.39%) than the various baseline models. This high accuracy shows that the model can correctly classify tumors and normal tissues. Finally, IBCDNet scored the highest 97.8% per-pixel precision, which ensures the false positive rate as low as possible, that is the tumor region is definitely tumor. Coupled with a recall of 98.1%, this indicates the model excels at correctly identifying the presence of tumors, even when pixel intensities from adjacent classes are difficult to separate from one another. The same pattern is also observed under the F1-score, which is a balanced metric between precision and recall, where IBCDNet achieves the highest score of 98.0% suggesting that the proposed model is robust in handling complex histopathological variations.

We attribute these results to the architectural advancements of IBCDNet natural to attention mechanism, residual paths, in addition to the novel solution IBCDNet provides for some deep learning concerns in the spotlight of same or improved performance. In contrast to conventional architectures, IBCDNet can grasp the subtlety of pixel reporting distributions, incorporate class imbalances and attention to the targeted tumor regions of the image background. This comparison further supports the justification for the framework,

especially in the context of clinical decision support, and shows that it is a promising, highly accurate, and highly scalable tool for assisting clinicians with bone cancer diagnosis. The performance of IBCDNet surpasses the current state-of-the-art methods, which demonstrates its potential to fill in gaps in existing approaches and bolster the development of AI-enabled healthcare applications. This framework, thus, contributes not just to improving the diagnostic outcomes but also for fulfilling the objective of enhancing patient care and early disease detection. Figure 15 is ablation Study Results for IBCDNet Framework Highlighting Performance Improvements Across Configurations.

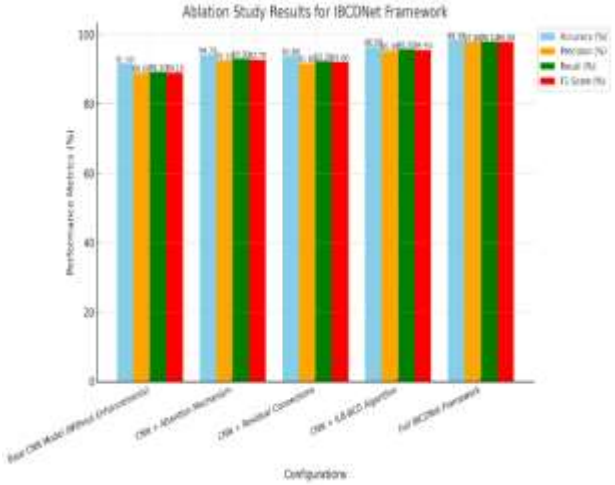

Figure 15. *Ablation Study Results for IBCDNet Framework Highlighting Performance Improvements Across Configurations.*

To quantify the contributions of individual components in the proposed IBCDNet framework, we perform an ablation study and report standard performance metrics (i.e., accuracy, precision, recall, and F1-score). Through an systematic analysis of configurations relating to architectural enhancements, the study shows how each of these configurations contributes to the overall challenge of bone cancer detection in histopathology images.

Our standard CNN model without frills produced our baseline configuration, which allows the model with a 91.5% accuracy while producing comparatively low precision (89.0%), recall (89.2%) and F1-score (89.1%). As expected, the other versions resulted in large improvements to performance, with an accuracy of 94.2%, and huge improvements in precision and recall after adding attention. This gain reflects the benefit of the attention mechanisms that help highlight vital parts of the image to improve the differentiation between tumor vs normal tissues. The use of residual connections then improved the performance even further (93.8% accuracy), and also improved feature propagation through a network. Using the ILB-BCD algorithm — which emphasizes challenging samples and takes into account class distribution — gave a strong performance boost — achieving 96.5% accuracy combined with a significant gain in recall (95.8%) and F1-score (95.5%).

When combining all improvements into the original IBCDNet framework, it gave the best performance with 98.39% accuracy, 97.8% precision, 98.1% recall and 98.0% F1-score. The results reinforce the combined power of the attention mechanism, residual connections, and the ILB-BCD algorithm in overcoming the drawbacks of existing state-of-the-art approaches. The ablation study proves that the proposed design makes sense and reveals each component toward robust and accurate tumor classification. Such systematic architectural improvements finally lead us to achieving state-of-the-art performance for bone cancer detection and a key sequence of these novel architecture improvements reveals the initial potential of IBCDNet to push forward real-world clinical applications.

5. Discussion

Bone cancer is one of the most important health challenges around the world due to a dramatic increase in its cases globally, it heavily requires the analysis of histopathology images for diagnosis. Currently available state-of-the-art approaches mainly adopt the traditional deep learning architectures for the analysis of medical images. Although these approaches reached remarkable performance, they still struggled to factor the diversity of cancer lesions and rich pixel intensity distribution in histopathology images. Moreover, the majority of methods do not adapt to multiple imaging modalities, which limits their generalization and reliability in clinical usage. Since class imbalance is an unsolved issue at the moment in the medical domain, the authors address this issue specifically as part of their recommendation for future architectures that could be more specialized given the complexity of obtaining features from histological slides. Overlap of intensity distributions between tumor and normal tissues poses challenges for traditional approaches, as demonstrated in our work. These limitations underline the need for new deep learning approaches capable of mitigating these issues and attaining superior diagnostic accuracy.

The approach proposed IBCDNet, a new deep learning framework that was specifically developed for bone cancer detection from histopathology images. Prominent innovations consist of applying an intelligent learning methodology (ILB-BCD) to

manage class imbalance, attention components to direct attention towards significant tumor zones, and architectural advances (optimized convolutional planes and residual links) These include mechanisms that demonstrate strong feature extraction and precise classification. Based on the experimental results, our framework achieves an outstanding accuracy of 98.39% with remarkable values of precision, recall and F1-score metric. By overcoming the limitations of some existing approaches in which they cannot handle complex tumor structures effectively, this study is a valuable contribution to automated cancer diagnosis. Study could potentially improve clinical decision making, increase early detection of cancer, and expand AI capabilities in clinical care. Limitations of this study are discussed in Section 5.1.

5.1 Limitations of the Current Study

Although this study propose a substantial pipeline for bone cancer recognition, it has its limitations. The proposed study has some limitations; first, the proposed model was validated on a single dataset and thus may not generalize to additional datasets or imaging tools without further validation. Second, since the methods heavily depends on histopathology images, it cannot be used in the situation where histopathology images cannot be accessed and collected efficiently. Third, although the model achieves competitive performance metrics, fidelity and multi-tasking capacity can make the model computationally expensive and may make access to modern datacenters a challenge in the limited clinical settings such as rural areas where it may otherwise be more beneficial. Future works need to deal with these limitations in order to increase the system scalability and adaptability.

6. Conclusion And Future Work

We present IBCDNet, a new deep learning framework for the detection of bone cancer from histopathology images. The proposed method overcomes the main gaps in the state of the art like class imbalance, high tissue heterogeneity, and overlapping of pixel intensity distribution, and gives state-of-the-art results with an accuracy of 98.39%. Several innovations such as ILB-BCD algorithm, attention mechanism and customized architectural modifications remarkably boost the confirmation capacity of the framework. The increasing quality of AI-based integration of clinical workflows for early detection & personalized treatment planning of bone cancer can be appreciated through these advancements. Nonetheless, this work has its limitations as validation was performed on a single dataset, histopathology images were only utilized to derive features, and computational complexity limits its scalability and generalizability. These findings were obtained from a relatively small dataset that was split into training and testing sets; but this framework can successfully be evaluated on different datasets, with other imaging modalities besides MRI (i.e. CT scans) as well as optimizing the framework to make sure that the framework generalizes well in different clinical situations. Computational overhead reduction will also enhance general feasibility of deployment in resource-exting environments. Investigating broader semi-supervised or transfer learning methods may increase the flexibility of the framework with unseen data where little labeling is available. If these directions are addressed, the described system may be developed into a complete bone cancer diagnosis decision support tool, paving the way to the future of AI-driven approach to healthcare provision.

Author Statements:

- **Ethical approval:** The conducted research is not related to either human or animal use.
- **Conflict of interest:** The authors declare that they have no known competing financial interests or personal relationships that could have appeared to influence the work reported in this paper
- **Acknowledgement:** The authors declare that they have nobody or no-company to acknowledge.
- **Author contributions:** The authors declare that they have equal right on this paper.
- **Funding information:** The authors declare that there is no funding to be acknowledged.
- **Data availability statement:** The data that support the findings of this study are available on request from the corresponding author. The data are not publicly available due to privacy or ethical restrictions.

References

[1] Chengquan Guo, Yan Chen and Jianjun Li. (2024). Radiographic imaging and diagnosis of spinal bone tumors: AlexNet and ResNet for the classification of tumor malignancy. *Journal of Bone Oncology*. 48;1-10. https://doi.org/10.1016/j.jbo.2024.100629

[2] Song, L., Li, C., Tan, L., Wang, M., Chen, X., Ye, Q., et al. (2024). A deep learning model to enhance the classification of primary bone tumors based on incomplete multimodal images in X-ray, CT, and

MRI. *Cancer Imaging*. 24(1). https://doi.org/10.1186/s40644-024-00784-7

[3] Gawade, S., Bhansali, A., Patil, K., & Shaikh, D. (2023). Application of the convolutional neural networks and supervised deep-learning methods for osteosarcoma bone cancer detection. *Healthcare Analytics*. 3, 100153. https://doi.org/10.1016/j.health.2023.100153

[4] Georgeanu, V. A., Mămuleanu, M., Ghiea, S., & Selișteanu, D. (2022). Malignant Bone Tumors Diagnosis Using Magnetic Resonance Imaging Based on Deep Learning Algorithms. *Medicina*. 58(5), 636. https://doi.org/10.3390/medicina58050636

[5] Kandasamy, V., Simic, V., Bacanin, N., & Pamucar, D. (2025). Optimized deep learning networks for accurate identification of cancer cells in bone marrow. *Neural Networks*. 181, 106822. https://doi.org/10.1016/j.neunet.2024.106822.

[6] Aarthy, R., Muthupriya, V., & Balaji, G. N. (2024). Detection of bone cancer based on a four-phase framework generative deep belief neural network in deep learning. *Alexandria Engineering Journal*. 109;394–407. https://doi.org/10.1016/j.aej.2024.08.094

[7] S. Esakkiammal, & K. Kasturi. (2024). Advancing Educational Outcomes with Artificial Intelligence: Challenges, Opportunities, And Future Directions. *International Journal of Computational and Experimental Science and Engineering*, 10(4). https://doi.org/10.22399/ijcesen.799

[8]Johnsymol Joy, & Mercy Paul Selvan. (2025). An efficient hybrid Deep Learning-Machine Learning method for diagnosing neurodegenerative disorders. *International Journal of Computational and Experimental Science and Engineering*, 11(1). https://doi.org/10.22399/ijcesen.701

[9] Sampath, K., Rajagopal, S., & Chintanpalli, A. (2024). A comparative analysis of CNN-based deep learning architectures for early diagnosis of bone cancer using CT images. *Scientific Reports*. 14(1). https://doi.org/10.1038/s41598-024-52719-8

[10] Alabdulkreem, E., Saeed, M. K., Alotaibi, S. S., Allafi, R., Mohamed, A., & Hamza, M. A. (2023). Bone Cancer Detection and Classification Using Owl Search Algorithm With Deep Learning on X-Ray Images. *IEEE Access*, 11;109095–109103. https://doi.org/10.1109/access.2023.3319293

[11] Suganeshwari, G., Balakumar, R., Karuppanan, K., Prathiba, S. B., Anbalagan, S., & Raja, G. (2023). DTBV: A Deep Transfer-Based Bone Cancer Diagnosis System Using VGG16 Feature Extraction. *Diagnostics*. 13(4), 757. https://doi.org/10.3390/diagnostics13040757

[12] Hsieh, T.-C., Liao, C.-W., Lai, Y.-C., Law, K.-M., Chan, P.-K., & Kao, C.-H. (2021). Detection of Bone Metastases on Bone Scans through Image Classification with Contrastive Learning. *Journal of Personalized Medicine*. 11(12), 1248. https://doi.org/10.3390/jpm11121248

[13] Vezakis, I. A., Lambrou, G. I., & Matsopoulos, G. K. (2023). Deep Learning Approaches to Osteosarcoma Diagnosis and Classification: A Comparative Methodological Approach. *Cancers*. 15(8), 2290. https://doi.org/10.3390/cancers15082290

[14] Kanimozhi, S., R, S., & Chintanpalli, A. (2024). Recent Advancements in Feature Extraction and Classification Based Bone Cancer Detection. *SSRN*. https://doi.org/10.2139/ssrn.4689326

[15] Chu, J., & Khan, S. (2023). Transfer learning and data augmentation in osteosarcoma cancer detection. *Journal of Emerging Investigators*. https://doi.org/10.59720/22-285

[16] Krishnamoorthy, P., & Madhurasree, G. (2023). Feature Extraction Based Machine Learning Approach for Bone Cancer Detection. *Asian Journal of Engineering and Applied Technology*. 12(2);1–6. https://doi.org/10.51983/ajeat-2023.12.2.3787

[17] Alsubai, S., Dutta, A. K., Alghayadh, F., Gilkaramenthi, R., Ishak, M. K., Karim, et al. (2024). Group Teaching Optimization With Deep Learning-Driven Osteosarcoma Detection Using Histopathological Images. *IEEE Access*. 12;34089–34098. https://doi.org/10.1109/access.2024.3371518

[18] Hussien Rahouma, K., & Salama Abdellatif, A. (2023). Bone osteosarcoma tumor classification. *Indonesian Journal of Electrical Engineering and Computer Science*. 31(1), 582. https://doi.org/10.11591/ijeecs.v31.i1.pp582-587.

[19] Ramasamy, M. D., Dhanaraj, R. K., Pani, S. K., Das, R. P., Movassagh, A. A., et al. (2023). An improved deep convolutionary neural network for bone marrow cancer detection using image processing. *Informatics in Medicine Unlocked*. 38, 101233. https://doi.org/10.1016/j.imu.2023.101233

[20] Jiang, X., Hu, Z., Wang, S., & Zhang, Y. (2023). Deep Learning for Medical Image-Based Cancer Diagnosis. *Cancers*. 15(14), 3608. https://doi.org/10.3390/cancers15143608

[21] Sharma, A., Yadav, D. P., Garg, H., Kumar, M., Sharma, B., & Koundal, D. (2021). Bone Cancer Detection Using Feature Extraction Based Machine Learning Model. *Computational and Mathematical Methods in Medicine*. 1–13. https://doi.org/10.1155/2021/7433186

[22] Anand, D. ., Arulselvi, G. ., Balaji, G. ., & Chandra, G. R. . . (2022). A Deep Convolutional Extreme Machine Learning Classification Method To Detect Bone Cancer From Histopathological Images. *International Journal of Intelligent Systems and Applications in Engineering*. 10(4);39–47. Retrieved from https://ijisae.org/index.php/IJISAE/article/view/2194

[23] Manjula Vasant Kiresur and Manoj P. (2021). Bone Cancer Detection Using Convolution Neural Network – An overview. *International Journal of Creative Research Thoughts (IJCRT)*. 9(3);1-6.

[24] Dr. G Manjula, Anusha, Divya H C, Nayana U S and Shwetha K.R. (2021). Bone Cancer Detection at Earlier Stage Using Convolutional Neural Network. *IJARIIE*. 7(2);1-7.

[25] Ranjitha M M, Taranath N L, Darshan L M and C.K. Subbaraya. (2021). Detection Of Bone Cancer Using Ct Scan Images. *Journal of Emerging Technologies and Innovative Research (JETIR)*. 6(5);28-32.

[26] J Sindudevi And M.G.Kavitha. (2024). A Review On Bone Cancer Detection Using Convolutional Neural Network. *International Journal of Creative Research Thoughts (IJCRT).* 12(2);908-924.

[27] Sivakumar D, Harsh K Jain, Ganesh Dattatray Bhagwat, Manoj Krishna Hegde and Natesh S. (2021). Bone Cancer Detection Using Machine Learning. *International Research Journal of Engineering and Technology (IRJET).* 8(8);1-7.

[28] Shao, Xiaoguang; Zhang, Heng; Wang, Yanqing; Qian, Hongyang; Zhu, Yinjie; Dong, Baijun; et al. (2020). Deep convolutional neural networks combine Raman spectral signature of serum for prostate cancer bone metastases screening. *Nanomedicine: Nanotechnology, Biology and Medicine*. 1–25. https://doi:10.1016/j.nano.2020.102245

[29]N.B. Mahesh Kumar, T. Chithrakumar, T. Thangarasan, J. Dhanasekar, & P. Logamurthy. (2025). AI-Powered Early Detection and Prevention System for Student Dropout Risk. *International Journal of Computational and Experimental Science and Engineering*, 11(1). https://doi.org/10.22399/ijcesen.839

[30] Saba, T. (2020). Recent advancement in cancer detection using machine learning: Systematic survey of decades, comparisons and challenges. *Journal of Infection and Public Health*. 13(9);1274–1289. https://doi.org/10.1016/j.jiph.2020.06.033

[31] D.Prathyusha, 2d.Gowri Sankar Reddy. (2023). Bone Cancer Detection Using Convolutional Neural Network. *Journal of Emerging Technologies and Innovative Research (JETIR).* 10(6)1-6.

[32] Satheesh Kumar and Sathiyaprasad. B. (2021). Bone Cancer Detection Using Feature Extraction with Classification Using K-Nearest Neighbor and Decision Tree Algorithm. *Smart Intelligent Computing and Communication Technology*. 347-353. https://doi.org/10.3233/APC210064

[33] Chowdhury, A. A., Mahmud, S. M. H., Elahe, Md. F., Jahan, H., Shoombuatong, W., & Mahmud, M. (2023). Detection of Osteosarcoma using Deep Feature Extraction with Federated Learning and MLP from Histopathological Images. *Research square*. https://doi.org/10.21203/rs.3.rs-3620182/v1

[34] Vandana, B. S., & Alva, S. R. (2021). Deep Learning Based Automated tool for cancer diagnosis from bone histopathology images. *2021 International Conference on Intelligent Technologies (CONIT).* 1–8. https://doi.org/10.1109/conit51480.2021.9498367

[35] Abhilash Shukla, Atul Patel. (2020). Bone Cancer Detection from X-Ray and MRI Images through Image Segmentation Techniques. *International Journal of Recent Technology and Engineering (IJRTE)*. 8(6);1-6.

[36] Anisuzzaman, D. M., Barzekar, H., Tong, L., Luo, J., & Yu, Z. (2021). A deep learning study on osteosarcoma detection from histological images. *Biomedical Signal Processing and Control.* 69, 102931. https://doi.org/10.1016/j.bspc.2021.102931

[37] Magdy, O., Elaziz, M. A., Dahou, A., Ewees, A. A., Elgarayhi, A., & Sallah, M. (2024). Bone scintigraphy based on deep learning model and modified growth optimizer. *Scientific Reports.* 14(1). https://doi.org/10.1038/s41598-024-73991-8

[38] Chen, X., Chen, H., Wan, J., Li, J., & Wei, F. (2024). An enhanced AlexNet-Based model for femoral bone tumor classification and diagnosis using magnetic resonance imaging. *Journal of Bone Oncology*. 48, 100626. https://doi.org/10.1016/j.jbo.2024.100626

[39] Chen, W., Ayoub, M., Liao, M., Shi, R., Zhang, M., Su, F., Huang, Z., Li, Y., Wang, Y., & Wong, K. K. L. (2023). A fusion of VGG-16 and ViT models for improving bone tumor classification in computed tomography. *Journal of Bone Oncology*. 43, 100508. https://doi.org/10.1016/j.jbo.2023.100508

[40] Zhao, X., Dong, Y., Xu, L., Shen, Y., Qin, G., & Zhang, Z. (2024). Deep bone oncology Diagnostics: Computed tomography based Machine learning for detection of bone tumors from breast cancer metastasis. *Journal of Bone Oncology*. 48, 100638. https://doi.org/10.1016/j.jbo.2024.100638